frontiers | Frontiers in Marine Science

TYPE Original Research
PUBLISHED 17 April 2023
DOI 10.3389/fmars.2023.1143982

OPEN ACCESS

EDITED BY
Hermano Melo Queiroz,
University of São Paulo, Brazil

REVIEWED BY
Laís Jimenez,
University of São Paulo, Brazil
Ruifeng Zhang,
Shanghai Jiao Tong University, China

*CORRESPONDENCE
Lei Gao
gaolei2009605@163.com
Xiancai Lu
xcljun@nju.edu.cn

†These authors have contributed equally to this work and share first authorship

SPECIALTY SECTION
This article was submitted to Marine Biogeochemistry, a section of the journal Frontiers in Marine Science

RECEIVED 13 January 2023
ACCEPTED 30 March 2023
PUBLISHED 17 April 2023

CITATION
Qi Z, Gao L, Chen D, Wang X, Liu H, Yang Y, Zhao Y and Lu X (2023) Vertical distribution of Fe, P and correlation with organic carbon in coastal sediments of Yellow Sea, Eastern China. *Front. Mar. Sci.* 10:1143982. doi: 10.3389/fmars.2023.1143982

Vertical distribution of Fe, P and correlation with organic carbon in coastal sediments of Yellow Sea, Eastern China

Zizhen Qi[1†], Lei Gao[1*†], Daixing Chen[1], Xuhao Wang[1], Huan Liu[2], Yang Yang[1], Yulian Zhao[3] and Xiancai Lu[2*]

[1]School of Marine Science and Engineering, Nanjing Normal University, Nanjing, Jiangsu, China, [2]Key Laboratory of Surficial Geochemistry, Ministry of Education, School of Earth Science and Engineering, Nanjing University, Nanjing, Jiangsu, China, [3]Key Laboratory of Solid Waste Treatment and Resource Recycling, Ministry of Education, Mianyang, Sichuan, China

The coastal zone is considered as a major carbon pool. Iron minerals and phosphates are vital factors affecting the amounts and occurrence of total organic carbon (TOC) in sediments. However, coupling mechanisms of iron (Fe) and phosphorous (P) in the source-sink transition of TOC in coastal sediments is poorly understood. This study characterized the distribution of Fe, P and TOC contents of three independent 170 cm sediment cores sampled from a coastal aquaculture area in the eastern Jiangsu Province, and quantified the correlations among Fe, P, median grain diameter (Dx(50)), and TOC. The results showed total phosphorus (TP) content ranges in a scope of 337.4-578.0 mg/kg, and many depths recorded moderate P eutrophication. Inorganic phosphorus (DA + IP) and biogenic apatite were the primary components of TP, accounting for 25.19–55.00 and 26.71–49.62%, respectively. The Fe contents varied from 987.9 mg/kg to 2900.7 mg/kg, in which oxidized iron (Fe_{ox}) accounted for about 62.2–79.4%. In the vertical profile, the TOC was positively correlated with the contents of low-crystallinity Fe-bearing carbonates (Fe_{carb}), high crystallinity pyrite (Fe_{Py}), iron-bound phosphorus (P_{CDB}), manganeses (Mn), and nitrogen (N), while it was negatively correlated with DA + IP, organic phosphorus (OP), and Dx(50). Based on the the partial least squares (PLS) model, we proposed that the higher Fe_{Py}, Mn, magnetite (Fe_{Mag}), Fe_{carb}, P_{CDB}, amorphous exchangeable Fe (Ex-Fe), and authigenic apatite phosphorus (Bio-P) in sediments represent the high capacity for TOC sink, whereas, higher DA + IP, and OP indicate a TOC conversion to the source. The non-siginificat indication of Fe_{ox} on TOC source-sink is due to its surplus and strong reactivity relative to TOC content. These revealed correlations provide a theoretical reference for understanding and regulating the burial rate and storage of TOC by changing the input of Fe minerals and P components into coastal sediments.

KEYWORDS

phosphorus, iron minerals, total organic carbon, correlation, coastal sediments

Highlights

(1) Characterized the vertical speciations of Fe and P in coastal sediments

(2) Established the indicated relationship between different Fe and P speciations and TOC source-sink

(3) Higher content of Fe_{carb}, Fe_{Py}, Fe_{Mag}, Ex-Fe, Mn, P_{CDB}, and Bio-P represent TOC sink.

(4) Higher content of DA + IP, and OP indicate TOC source.

(5) Non-siginificat indication of Fe_{ox} on TOC source-sink is due to its surplus and strong reactivity.

1 Introduction

Marine "blue carbon" refers to the carbon sequestrated and stored in biomass and sediments by the oceans and coastal ecosystems (Tang et al., 2018; Macreadie et al., 2019; Macreadie et al., 2021). The contribution made by the coastal carbon pool accounts for ~99% of the final blue carbon sink (Tang et al., 2018). Some of the organic carbon is re-released or converted into CO_2 as a carbon source again through microbial metabolic activities (Zhang et al., 2017). The storage of organic carbon and inert carbon in the sediment is an important contributor to the carbon sink (Jiao et al., 2014). The "source-sink" of the coastal zone carbon pool fluctuates with the change of redox conditions due to hydrodynamics (Xu et al., 2021), terrigenous input, mineral conversion, and eutrophication. Various minerals have been widely believed to be important to promote the persistence and sink of organic carbon in sediments (Hemingway et al., 2019; Kleber et al., 2021). In particular, most of the iron and manganese minerals in sediments have large specific surface areas and high redox sensitivity, which can permanently preserve organic carbon through adsorption and surface complexation (Giannetta et al., 2020; Bao et al., 2022), as well as surface precipitation (Du et al., 2018). There is also a significant correlation between the sequestration and release of TOC with phosphorous (Huang et al., 2016; Fang and Wang, 2021). Phosphorous can accelerate TOC degradation directly or indirectly by enhancing microbial activities (Jiao et al., 2010). Meanwhile, phosphorus addition can directly improve TOC stability by increasing aggregate particle size and indirectly affect TOC stability by increasing Fe oxide form conversion in sediments (Du et al., 2022). The redox conditions of the coastal sediments commonly fluctuate greatly, different Fe oxide and phosphorus forms are very sensitive to it, and phosphorus eutrophication is serious due to terrestrial input (Singh et al., 2021). Therefore, phosphorous and Fe oxides and their special transformation are the key factors affecting TOC sequestration in coastal sediments.

In sediments, the interaction between minerals and organic matter occurs preferentially on specific minerals; therefore, the mineral composition is a crucial factor for the sequestration of organic matter (Hedges and Keil, 1995; Kleber et al., 2021). Many studies have proven that Fe minerals are important carriers of organic carbon in terrestrial soil (Sarkar et al., 2018; Kleber et al., 2021), and in the ocean sediment (Zhao et al., 2023). Fine-grained components in coastal sediments positively correlated with the contents of unstable minerals (Cao et al., 2018), especially the contents of Ca/Mg-rich carbonates with poor stability (Fookes and Higginbottom, 1975; Yalcin et al., 2022). Although the abundance of Fe minerals in coastal sediments is not as high as that of carbonates, the promotion by Fe oxides on the storage of organic matter through surface precipitation and adsorption has been well recognized (Canfield, 1994). An onion-like structure with encapsulated organic matter in iron minerals formed due to the diffusion and aggregation of iron and carbon, which weakens the decomposition of organic matters by microorganisms (Lalonde et al., 2012). Recently, scientists have proposed that the current hypothesis that the mineral matrix has a protective mechanism for TOC is simplistic, and the spatial and functional complexity of the mineral-organic matter should be considered (Yalcin et al., 2022). And study pointed that mineral–organic preservation is an important missing process in current assessments of Earth's long-term carbon cycle (Zhao et al., 2023). Hence, analyzing the correlation between the occurrence of organic carbon in the sedimentary profile of coastal zone and the occurrence of iron and manganese minerals is crucial to determine their contribution to the "carbon sink" of "blue carbon".

Phosphorus is also a key player in the geochemical cycle of TOC (Arif et al., 2021) and is easily fixed or affected by Fe minerals (März et al., 2018). The leading states of phosphorus nutrients in marine sediments include exchangeable, organic, iron-bound, autoecological apatite, detrital, and refractory organic (Fang and Wang, 2021), two-thirds of which are related to poorly crystalline iron and manganese oxides (Hermans et al., 2021). In aquatic and terrestrial systems, the interaction between phosphate and ferric oxides typically involves adsorption/desorption (Boujelben et al., 2008; Yoon et al., 2014), precipitation/dissolution of surface Fe-phosphate phases (Weng et al., 2012), and precipitation of phosphate in iron (III) oxides (Cheng et al., 2015; März et al., 2018). On the one hand, several iron minerals were found capable of promoting the hydrolysis of phosphate (Li et al., 2020). Significantly, Ca-bearing iron minerals could enhance the hydrolysis of phosphate by promoting the precipitation of calcium phosphate minerals (Wan et al., 2021). In turn, the interaction between phosphate and Fe(III) oxide significantly affects the mineralization pathway of the Fe phase, e.g., the presence of phosphate is a crucial factor for the formation of green rust during the reduction of hematite by iron-reducing bacteria (IRB) (O'loughlin et al., 2015). According to a statistic of iron minerals with different genesises, approximately 10% of phosphate in sediments remobilized into the pore fluids due to IRB activities (Schad et al., 2021). Hence, reactive P phases are therefore invoked as regulatory factor for Fe mineral transition and bounded with carbon source-sink under the driving effect of microbial remineralization.

In this study, we analyzed the total organic carbon, geochemical characteristics, and different forms of Fe oxides/minerals and phosphorus of sediment cores sampled from a coastal site of the Yellow Sea, Jiangsu Province, Eastern China. Based on Spearman's

multi-element correlation analysis, cluster analysis, and partial least squares (PLS) model, this study quantifies the correlation between median particle size (Dx(50)), Fe/Mn, P, and TOC in the profile. After that, the significant impact of human activities on the mechanisms of carbon sequestration by inducing the transformation of Fe minerals is discussed. Compared with previous studies, this paper presents the following contributions: (1) Characterized the distribution of Fe, P speciations and TOC contents in a sedimental of 170 cm core to further refine the occurrence of iron minerals and phosphorus in profile coastal; (2) Established correlation between TOC and Fe, P speciations based on Spearman's multi-element correlation analysis to deeply understand the complicated relationships between TOC and different Fe, P speciations; (3) Predicted the primary and secondary factors on affecting TOC source-sink transition based on the partial least squares (PLS) model to catch on carbon source-sink mechanism in coastal sediments.

2 Materials and methods

2.1 Sampling of sediments

In October 2021, sediments were collected from a marine mudflat in Bencha Town, Rudong, Nantong, Jiangsu Province (32°35'19.0422' N, 120°54'47.2608' E) (Figure 1). Bencha town is an important coastal aquaculture area. The sampling area was transition zone for aquaculture discharge from terrigenous to sea. Three profiles of 1.7 m in depth were excavated at adjacent three points. The samples were split every 10 cm in the profiles and were immediately put into sterile sealing bags, and there were 51 sample in total (17 samples/profiles sediment core). After emptying the air, the samples were quickly put into a foam box and frozen with dry ice. The boxes were transported back to the laboratory on the same day for cryopreservation at –80°C. In the lab, the sealing bags containing sediment were melted at 4°C, a certain amount of samples were divided into 50 ml centrifuge tubes in an anaerobic glove box, and then freeze-dried, grounded with an agate mortar and passed through a 200-mesh sieve for further analysis, including the sequential extraction of iron and phosphorus, measurement of total organic carbon (TOC) and nitrogen (N), and analysis related geochemical indexes. Meanwhile, 100 g wet sample was divided into in 250 ml centrifugal cup and centrifuged at high speed refrigerated centrifuge (6000 r/min, 20 min) to extract pore water, the supernatant liquid was filtered through a 0.45 μm microporous membrane. The chemical pH of the extract pore water were measured using a pH meter (Thermo Fisher, Star A2110). Other samples were used for analysis of grain size and microscopic observation.

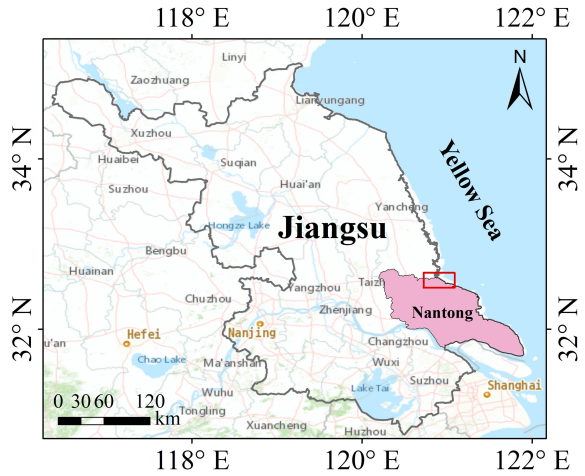

FIGURE 1
Map of the location of the study area.

2.2 Analysis of grain size of sediments

The grain size distribution of sediments was analyzed by using a Mastersizer 3000 laser grain-size analyzer (Shanghai, China). The measurement range was 0.02–2000 μm, and the relative error was less than 2%. The specific steps were as follows: 0.5 g of samples were placed in a 100 ml beaker, and 10 ml of mass fraction 10% of hydrogen peroxide (H_2O_2,CAS, 7722-84-1) was added to remove the organic matter in the sediment sample, and then 10 ml of mass fraction 10% hydrochloric acid (HCl, CAS, 7647-01-0) was added to remove the calcium cements. Next, the samples were sufficiently washed to neutralize them. Subsequently, 10 ml of 1 M sodium hexametaphosphate ($Na(PO_3)_6$, CAS, 68915-31-1) was added and placed in an ultrasonic oscillator to disperse the samples for grain size distribution analysis. The grain size ranges of clay, silt and sand were followed previous study by < 4 μm, 4–63 μm, and > 63 μm, respectively. Dx(50) was used to represent the median grain diameter of the sediment samples (Trefethen, 1950). All above chemical reagents were analytical reagent which purchased from Merck Limited Company (Shanghai, China).

2.3 X-ray fluorescence spectrometer (XRF) analysis

The abundance of major and trace elements was measured using a X-ray fluorescence analysis (Epsilon 3, PANalytical). The freeze-dried samples were pressed into pieces mixed with boric acid. And the pieces were scanned for 30 s with a step of 5 mm to acquire XRF spectra. The relative abundances of 8 significant and 26 trace elements were then calculated based on the collected spectra.

2.4 Analysis of carbon/nitrogen contents of sediments

The CN model of the Vario Max elemental analyzer (Elementar Analysensysteme GmbH) was used to test total carbon (TC), TOC, and nitrogen with an analysis error of less than 0.03%. Here 3 g pre-treated samples were placed in the sealed bags to measure the total content of carbon (TC), which includes the carbon in organic and inorganic states. Meanwhile, another 3 g pretreated samples was added with appropriate amount of 2 M HCl and shook for 48 h to

fully remove the inorganic carbon. Then, the samples with the additives were centrifuged at 3500 g, and the filter cakes were washed with ultrapure water five times, and finally freeze-dried. The acid-treated samples were placed in the sealed bags to measure the total content of carbon, which represents TOC. Therefore, the total inorganic carbon content (TIC) can be calculated by subtracting TOC from TC (TIC = TC-TOC). Calculated carbon ratio to nitrogen (C/N) by TC/N which was used to track source of organic matter.

2.5 Extraction and analysis of different speciations of iron in sediments

The five-step sequential extraction of different forms of iron was completed with little modified according to methods described in the literature (Poulton and Canfield, 2005). 0.1 g freeze-dried samples were weighted for the extraction. First, exchangeable Fe (Ex-Fe) was extracted by using 1 M $MgCl_2$. Second, low-crystallinity Fe-bearing minerals, such as iron sulfide, ferrous carbonate (calcite and dolomite), and easily reducible Fe oxides (ferrihydrite and lepidocrocite), were dissolved by using 1 M HCl to extract Fe_{carb}. Third, 0.35 M acetic acid, 0.2 M sodium citrate, and 50 $g{\cdot}L^{-1}$ sodium dithionite were mixed to the selective extraction of reducible oxides (goethite, hematite and akagane´ite) and reducible iron oxide (Fe_{ox}), including goethite, hematite, ferrihydrite or lepidocrocite. Fourth, magnetite (Fe_{Mag}) with high crystallinity was extracted by using 0.2 M oxalic acid or 0.17 M ammonium oxalate. Finally, the ferrous species in Fe-bearing minerals with high crystallinity include pyrite, iron (oxyhydr) oxides, siderite, ankerite, and certain sheet silicate minerals (e.g. nontronite, chlorite, glauconite, biotite). The concentrated HNO_3 was used to extract the Fe accommodated in these minerals, which is denoted by Fe_{Py}. The extraction of manganese hosted in iron minerals was carried out synchronously, and the final manganese content was the sum of the manganese content in five steps. The extract was diluted with 2% HNO_3 to make the Fe and Mn contents less than 2%, and was analyzed by inductively coupled plasma optical emission spectrometry (ICP-OES).

2.6 Extraction of different forms of phosphorus in sediments

0.1 g freeze-dried samples were placed in a centrifuge tube. According to the method described by Ruttenberg (1992), different forms of phosphorus were extracted in five steps. First, exchangeable or loosely sorbed phosphorus (Ex-P) was extracted by using 1M magnesium chloride. Second, iron-bound phosphorus (P_{CDB}) was extracted with CDB solution (0.30 M sodium citrate, 1.0 M $NaHCO_3$, pH 7.6, 1.125 $g{\cdot}L^{-1}$ sodium dithionite). Third, authigenic apatite, $CaCO_3$-bound P and biogenic apatite (Bio-P) were extracted by using sodium acetate solution. Fourth, 1M HCl was used to extract detrital apatite and other inorganic phosphorus (DA + IP). Finally, the samples were sintered at 550°C, and 1M HCl was used to extract the phosphorus, which represents organic phosphorus (OP). All of the final extracts were diluted to a salt content of less than 2% and then analyzed by using ICP-OES.

2.7 Scanning electron microscope (SEM) observation of iron minerals in sediments

Samples of freeze-dried sediments were dropped onto silicon wafers, and sputtered coating with Pt. A field emission-scanning electron microscope (SEM) (Carl Zeiss, Oberkochen, Germany) was used to observe Fe-Mn minerals. The energy dispersive spectrometer (EDS) (AZtecOne X-Max 150; Oxford Instruments, Abingdon, United Kingdom) equipped with SEM was used to measure the chemical composition of the minerals.

2.8 Correlation analysis of Fe-P-TOC

Spearman's correlation coefficient (one tail) analysis was performed using IBM SPSS Statistics 25 software to analyze the correlation between the mean grain size Dx (50) of iron, manganese, phosphorus, nitrogen, and total TOC. $P < 0.05$ was considered statistically significant. The K-means clustering classification principle divides similar samples into as many classes as possible (Nakamura et al., 2009). The R Core Team, 2022 (https://www.R-project.org/) was used to perform K-means clustering analysis on iron, manganese, phosphorus, nitrogen, Dx (50), and TOC to compare and analyze the factors in the same group as the TOC changes. The partial least squares (PLS) model associates two data matrices, X and Y, through a linear multivariate model, providing quantitative modeling of the complex relationship between the predictor variable X and response variable Y (Wold et al., 2001). For each PLS, the cumulative explained variation of Y (R^2) was calculated to evaluate whether the correlation was significant or not. The predictive squared correlation coefficient (Q^2) was used as the measure of robustness, and higher predictability was marked when it was larger than 0.50 (Golbraikh and Tropsha, 2002). SIMCA 14.1 was used to predict the partial least squares model to explore the relative importance of potential influencing factors of OC in Jiangsu coastal sediments. The ability of the independent variable to predict TOC and its importance to the dependent variable (Shi et al., 2014) rely on the variable importance of projection (VIP). Commonly, VIP > 1 indicates that the variables are able to predict the response variable. In contrast, VIP < 0.5 indicates that the relationship is less significant and should be removed from the model (Wold, 1995). Images were drawn using Origin 2018, R 4.1.3, CorelDRAW 2021 and online software available at https://www.chiplot.online/. All the data and standard deviations of each layer were obtained from the average of the three cores.

3 Results

3.1 Geochemical profile of sedimental components and TOC

The sediments are primarily composed by fine silt. With increasing depth, the median particle size overall decreased (Figure 2A). In the profile, the contents of sand, silt, and clay ranged from 5.05%–19.43%, 76.89%–89.86%, and 2.61%–6.37%. The silt content at most depths

exceeded 80% (Figure 2A), while the sand content was generally less than 17%. The pH of the pore water ranged from 7.45–8.48, with an average of 7.83. At depths of 40–50, 80–90, and 100–110 cm, the pH of the adjacent layers fluctuated (Figure 2B).

The TOC of sediments ranged from 1.03-2.10 g/kg, with an average of 1.44 g/kg (n = 51), a maximum at 100–110 cm, and a minimum at 120–130 cm. Its content is similar to that of most coastal zones(Fang and Wang, 2021; Xia et al., 2022), but it's significantly lower than that of terrestrial soil environment (Yan et al., 2021; Shi et al., 2022). The N was 0.20-0.44 g/kg, with a maximum at 160–170 cm and a minimum at 120–130 cm. The TOC/N ratio ranged from 3.32–6.32 with an average of 4.45 (n = 51). The TC/N ratio ranged from 22.04–46.27 with an average of 31.61 (n = 51), a maximum at 130–140 cm, and a minimum at 160–170 cm. The TOC/N ratio fluctuated significantly compared with the TC/N ratio, especially in the facultative anaerobic layer (30 cm) where redox conditions change greatly (Figure 2C). A TC/N ratio >12 indicates that the main source of organic matter is terrigenous organic matter, while a TC/N ratio between 6–9 indicates that the main source is the sea (Cifuentes et al., 1996). Therefore, the organic matter in the sediments here was mainly derived from terrestrial sources.

3.2 Vertical distribution of iron speciation

According to the sequential extraction of iron, the total iron content in the profile was scopes from 987.9 mg/kg to 2900.7 mg/kg. The reducible oxides Fe_{ox} was predominant (62.2%–79.4%), while the Fe_{carb}, Fe_{Mag}, and Fe_{Py} were 6.9%–17.9%, 6.6%–11.5%, and 4.1%–9.0%, respectively. The Ex-Fe content was the lowest, accounting for 0.5%–1.4%. Despite being low, the Ex-Fe content fluctuated the most with the depth (Figure 3). The Fe_{carb} content decreased with increasing depth, whereas Fe_{ox}, Fe_{Mag}, and Fe_{Py} accumulated gradually (Figure 3). Meanwhile, Mn content existed with extractable iron minerals increased with increasing depth, which might indicate that manganese was firstly dissolved and released into pore water, and then fixed by iron oxides as the iron minerals was reduced. At the profile bottom of 160–170 cm, iron oxide contents still were the highest, which may be due to microbial mineralization (Figure 3).

Based on SEM observation, Fe-rich or Mn-rich carbonate, iron oxides, and pyrite framboids were observed at the redox interface of 40–50 (Figure 4A) and 70–100 cm (Figures 4B–F), while Fe-rich clay minerals were the primary carrier minerals at depths of 130–140 (Figure 4G) and 160–170 cm (Figure 4H). At the redox interface at a depth of 40–50 cm, flaky iron-rich carbonates occurred along the edge of the sand matrix, such as the observed cubic regular crystalline iron-rich carbonates (Figure 4A), which is consistent with the observation of Kontny et al. (2021). However, at this depth, little manganese was detected in these iron carbonates (Figure S2-1). At depths of 70–80 cm, iron mineral species were abundant, including granular iron carbonates with high Mg and Mn adhered to the edge of the sand matrix (Figures 4B, C; Figure S2-4), pyrite framboids with diameter of about 5–20 μm (Figure 4D). Iron carbonates with higher Mg were also found at 80–90 cm (Figure 4E). At depths of 90–100 cm, the Fe-carbonate changed into plate-shape (Figure 4F) and contained much higher Mn content (Figure S2-6), the EDS analysis indicated the formation of siderite (Liu et al., 2019). We found there were Mg-rich siderite, Mg-Mn-rich siderite and Mn-rich siderite. The Mn-rich siderite likely formed at deep. Meanwhile, the SiO_2 particles became finer with increasing depth. At depths of 160–170 cm, various Fe-containing clays mainly occurred on the surface of the sandy matrix (Figure 4H). According to the XRF analysis (Figure 4I), the relatively high Mn contents were observed at the depths of 70–80, 110–110, and 160–170 cm.

3.3 Vertical distribution of phosphorus

The total phosphorus (TP) content in sediments ranged from 337.4–578.0 mg/kg, with an average of 454.4 mg/kg. Inorganic phosphorus was dominated (98.42%–99.99%), and organophosphorus content was relatively low (0.3–7.3 mg/kg). The Ex-P content was 3.3–3.7 mg/kg, only accounting for a very low proportion (0.58%–1.02%). With the increase of depth (<100 cm), Ex-P was released. The P_{CDB} content was 22.6–249.6 mg/kg, Bio-P content was 128.9–286.8 mg/kg, and detrital apatite plus other inorganic phosphorus (DA+IP) was 133.0–224.1 mg/kg, which accounted for 5.36%–47.28%, 26.71%–49.62%, and 25.19%–55.00% of TP content, respectively. The Bio-P and DA+IP were the main forms of phosphorus. The OP mainly distributed below 50 cm (Figure 5).

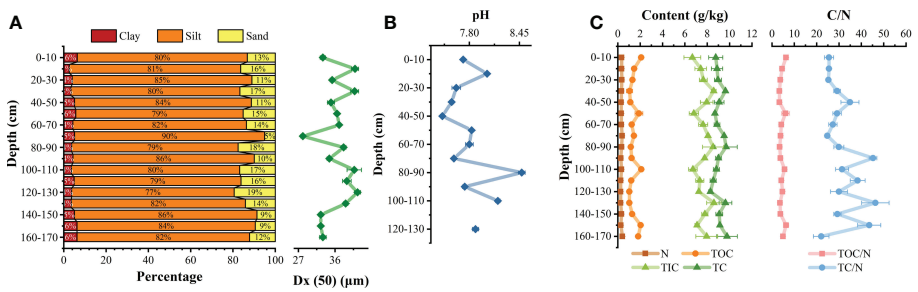

FIGURE 2
Vertical profile distribution of particle size of sediment **(A)**; vertical pH changes of pore water **(B)**; Changes of total organic carbon (TOC) and carbon ratio to nitrogen (C/N) **(C)**.

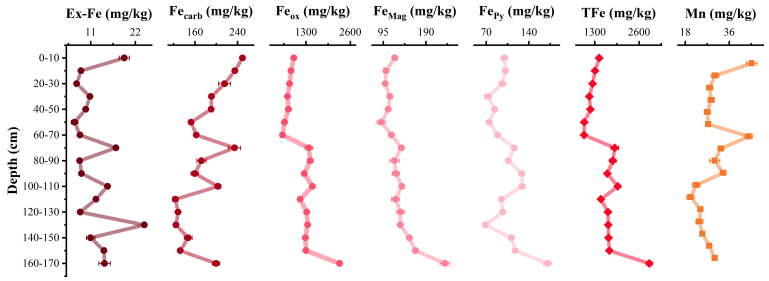

FIGURE 3
Distribution of different speciations of iron minerals at vertical profile. Ex-Fe represents exchangeable iron, Fe_{carb} represents low-crystallinity Fe-bearing carbonates, Fe_{ox} represents easy-reduced iron oxide, Fe_{Mag} represents high-crystallinity magnetite, Fe_{Py} represents high crystallinity. Non-reactive pyrite, TFe represents the total content of iron minerals, and Mn represents the occurrence of manganese hosted in iron minerals.

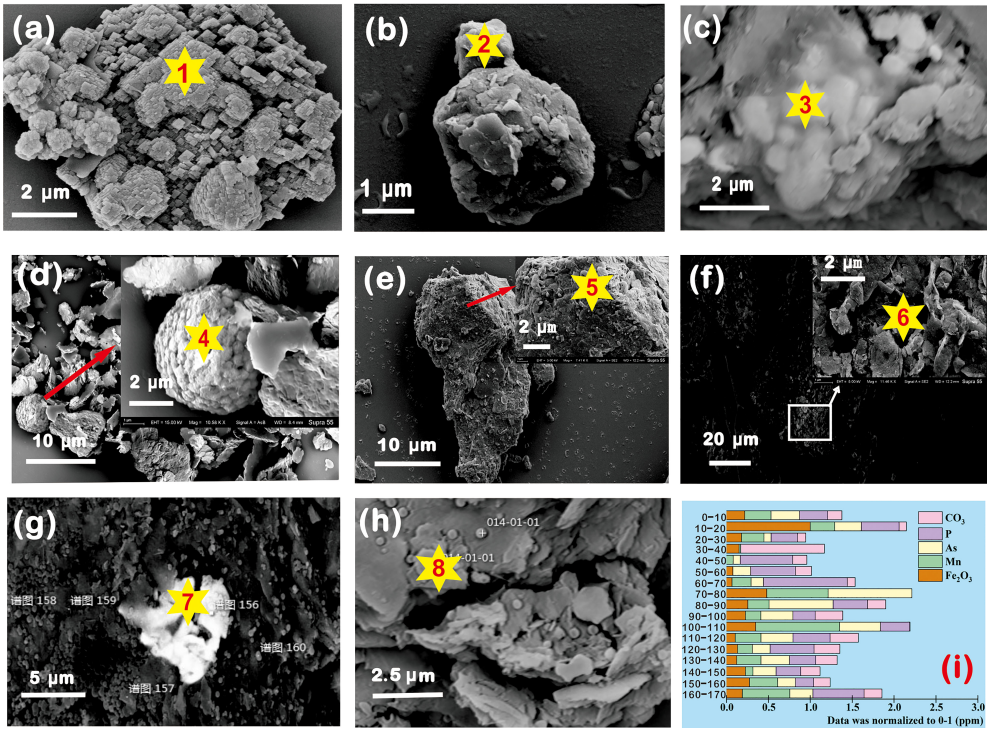

FIGURE 4
Emission-scanning electron microscope (SEM) images of different iron speciations in vertical profile. **(A)** : 40-50 cm; **(B–D)**: 70-80 cm; **(E)**: 80-90 cm; **(F)**: 90-100 cm; **(G)**: 130-140 cm; **(H)**: 160-170 cm and **(I)**: Normalized relative abundance of partial major elements based on X-ray Fluorescence Spectrometer data.

3.4 Correlation of TOC and clustering of the parameters

Using SPSS bivariate Spearman test results, TOC was positively correlated with Fe_{carb} (r = 0.495, P = 0.022), Fe_{Py} (r = 0.542, P = 0.012), Mn (r = 0.419, P = 0.047), P_{CDB} (r = 0.471, P = 0.028), and N (r = 0.554, P = 0.011) and negatively correlated with DA+IP (r = –0.427, P = 0.044) and Dx (50) (r = –0.418, P = 0.047) (Figure 6A; Table S2).

According to the K-means clustering analysis and TOC occurrence correlation index, the final clustering of relevant indicators produced three clusters. Ex-Fe, Mn, Ex-P, OP, N, Dx (50), Fe_{Py}, Fe_{Mag}, and P_{CDB} were in the same cluster as TOC (Figure 6B). Additionally, Fe_{carb}, DA+IP, and Bio-P were in the same cluster, TFe and Fe_{ox} were in the other cluster (Figure 6B).

4 Discussion

4.1 Correlation between TOC and iron states

Most studies have discussed the mechanism for stabilizing TOC by iron minerals in continent soil and in the lakes, salt marsh

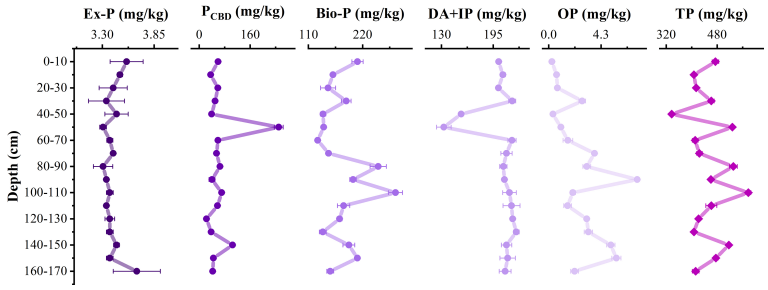

FIGURE 5
Distribution of different forms of phosphorus at vertical profile. Ex-P represents exchangeable or loosely sorbed phosphorus, P_{CDB} represents iron-bound phosphorus, Bio-P represents authigenic apatite, $CaCO_3$-bound P and biogenic apatite, DA+IP represents detrital apatite plus other inorganic phosphorus, OP represents organic phosphorus, and TP represents total phosphorus.

wetlands, or ocean sediments (Lalonde et al., 2012; Ma et al., 2018; Reichenbach et al., 2023; Zhao et al., 2023). The TOC sequestration controlled by iron minerals is complicated and strongly related to the redox conditions of sediments (Hartnett et al., 1998; Hemingway et al., 2019). While study pointed that mineral–organic preservation is an important missing process in current assessments of Earth's long-term carbon cycle (Zhao et al., 2023). Redox conditions of coastal sediments vary greatly in vertical profiles as terrigenous input (Anschutz et al., 2019), and Fe-carbonates are enriched commonly due to dynamic drive of the tide (Lapointe et al., 1992). Therefore, the correlation between different speciations of iron minerals (TFe, Ex-Fe, Fe_{carb}, Fe_{ox}, Fe_{Mag}, and Fe_{Py}) and TOC in the coastal sedimental profile is crucial for understanding the carbon sequestration and sink.

In our study, the spearman test indicates that TOC is positively correlated with Fe_{carb} and Fe_{Py} at 0.01 and 0.05 levels (Figure 6A). We observed Mn-Fe-rich carbonate minerals from the depth of 40–50 cm (Figure 4A, Figure S2-1), and Fe-carbonate with high Ca and Mg contents occurred at 80–90 cm (Figure 4C, Figure S2-4), which may be ferrodolomite (Wen et al., 2007). Fe-carbonate is generally formed in anaerobic sediments mediated by microbial dissimilatory and chemical reduction of Fe(III), accompanied by the transformation of organic matter (Lovley, 1991; Thamdrup, 2000). And high concentrations of goethite, limonite and sulfide, and small amounts of hematite and ferromanganese oxides are formed in the carbonate sediments (Ferguson et al., 1983). Recent studies suggested that the stability of TOC fixed by Fe_{carb} may be transformed due to Fe(III) reduction and Fe(II) oxidation, which will further affect the stability of TOC-Fe_{carb} (Ma et al., 2022). Therefore, we hold the opinion that the formation and occurrence of Fe_{carb} in sediments indicate TOC sink associated with symbiosis with more iron hydroxide.

The chemical zones in the sediment are named the top aerobic oxidation zone, nitrate reduction zone, manganese reduction zone, iron reduction zone, sulfate reduction zone, and methanogenesis zone in sequence (Treude et al., 2014). The type of some authigenic minerals (minerals formed after the detritus has sunk) can indicate REDOX conditions and pH (Kerr et al., 2018). At depths more than 60 cm, the extent of transformation of amorphous iron minerals to high crystalline minerals gradually increased. Pyrite framboids presented at a depth of 70–100 cm (Figure 4D) in the sulfate reduction zone and methanogenesis zone, and TOC content reached a peak of 2.10 g/kg at depths of 100–110 cm (Figure 2). Formation of pyrite occurred in the anoxic environment due to sulfate reduction (Sweeney and Kaplan, 1973; Canfield, 1989) and in methanogenesis zone coupled with sulfur to form pyrite (Wang et al., 2022). Earlier studies have

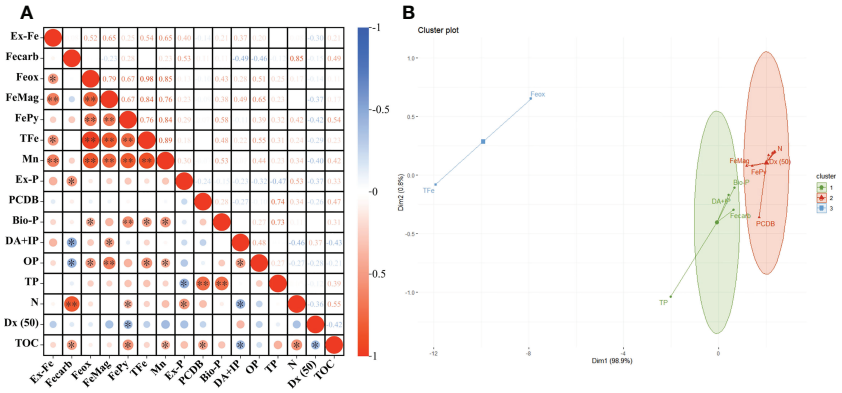

FIGURE 6
Correlation between TOC and different parameters of sediments. "*" and "**" indicated significant correlations at $P < 0.05$ level and $P < 0.01$ level respectively **(A)**. K-means clustering analysis results of different parameters **(B)**.

demonstrated that an increase in TOC inhibits the Formation of Fe exchange by decaying sulfate reduction in sediments (Raiswell and Canfield, 1998). So we suggested that Fe_{Py} indicates TOC sink in a redox range in which the accumulation of TOC is favored due to the low energy efficiency for its mineralization.

Recent reported that 25–62% of total reactive iron, which generally refers to exchangeable, low-crystallinity Fe-bearing minerals, reducible iron oxides (Canfield, 1989; Krom et al., 2002), are responsible for transferring a large quantity of TOC to the carbon sink (Barber et al., 2017). However, our study found that Fe_{ox} was not significantly correlated with TOC at 0.01 and 0.05 levels (Figure 6A), although the reducible oxides Fe_{ox} predominated 62.2%–79.4% in TFe (Figure 6A). The content of Fe_{ox} (0.98–2.99 g/kg) was surplus compared with TOC transition consumption (1.03-2.10 g/kg) and our analysis is that only part of Fe_{ox} participates in the oxidation transformation and stable preservation of TOC, so the indication absence of Fe_{ox} on TOC source-sink due to its abundance relative to TOC content. During coprecipitation of TOC with Fe_{ox}, TOC is sequestered *via* adsorption and incorporation with mineral particle (Lalonde et al., 2012). Multilayers of TOC or macromolecular OC-Fe complexes to preserve TOC when particle surfaces become saturated (Chen et al., 2014; Li et al., 2023). Previous study also reported that there was no correlation between TOC fractions and pH, Fe_{ox}(1.7-4.2 g/Kg), or Al oxides Al_{ox} (1.7-4.2 g/kg) in topsoils (0–20 cm) in subtropical China, while effects of Fe_{ox} on soil properties was significant (Mao et al., 2020), and the specific mineralogical properties and reactivity determine TOC stocks in tropical forest and cropland and was constrained by soil mineralogy (Reichenbach et al., 2023). In additional, recent study found that maybe only carboxyl-rich TOC coprecipitated with ferrihydrite becomes more stable in the solid phase (Zhao et al., 2022), and in turn TOC occurrence can delay the conversion of Fe (hydroxyl) oxide to iron minerals with higher crystallity (Pasakarnis et al., 2014). The content of Fe_{ox} (0.98–2.99 g/Kg) is not very surplus compared with TOC transition consumption (1.03-2.10 g/kg) (Figures 2, 3). Our analysis is that Fe_{ox} is very reactive, and only part of Fe_{ox} participates needed in the oxidation transformation and stable preservation of TOC. We suggested that the non-significant contribution of Fe_{ox} to on carbon sink–source in coastal sediments mainly related to surplus and strong reactivity.

For exchangeable iron (Ex-Fe) is metastable on geological time scales and is a crucial factor for long-term organic carbon storage (Lalonde et al., 2012). Large amounts of TOC in seafloor sediments have been shown to bind to Ex-Fe rather than be controlled by autogenic minerals (Faust et al., 2021). In this study, the Ex-Fe was only 0.5%–1.4% (Figure 3). However, TOC occurrence can delay the conversion of Fe(hydroxyl) oxide to iron minerals with higher crystallite and inhibits the electron transfer between the Ex-Fe in the liquid phase and Fe(III) in solid phase (Zhao et al., 2022). A previous report also suggested that carbon in the minerals may be more mobile and less stable than we previously thought due to iron minerals remaining dynamic and mixed with Ex-Fe in the surrounding liquid phase (Pasakarnis et al., 2014). So we maintained that Ex-Fe was also a vital TOC sink favor factor due to its conducive to the crystallization of iron minerals. Moreover, the low active iron Fe_{Mag}, Ex-Fe were grouped into the same category with Fe_{Py} and TOC in K-means cluster analysis (Figure 6B). So we suggested that Fe_{Mag} may be correlated with TOC sink as for its low activity.

In addition to Fe(III), Mn(III/IV) minerals strongly interact with organic matter in marine sediments (Johnson et al., 2015; Fang and Wang, 2021). The Mn content associated with extractable iron (987.9–2900.7 mg/kg) was about 20.8–46.2 mg/kg (Figure 3), and was positively correlated with TOC (Figure 6). K-means cluster analysis further shows that manganese and TOC were similar (Figure 6B), indicating that this occurrence of manganese contributed to the TOC deposition. Therefore, we propose that Ex-Fe, Fe_{carb}, Fe_{Py}, and manganese are favorable for organic carbon sink in coastal sediments. The correlation between TFe, Fe_{Mag}, Fe_{ox}, and TOC cannot be directly determined at the *P* value of 0.05 to 0.01 level (Figure 7).

4.2 Different forms of phosphorus correlated with TOC

Over the past 30 years, coastal aquaculture industries and terrestrial inputs have contributed to the eutrophication or over-eutrophication of the coastal environment (Smith and Schindler, 2009). According to Berbel et al. (2015), TP between 495–1300 mg/kg in estuarine sediments indicates moderate pollution. The TP extracted from the sediments in the studied area was 337.4–578.0 mg/kg, therefore, the TP status can be classified as moderate eutrophication. We found that Bio-P and DA+IP were the main contributors to sediment TP (Figure 5). DA+IP is predominantly from terrestrial weathering, whereas Bio-P is derived from fluorapatite phosphorus formed by biological metabolism, bioclastic mineralization, and early diagenesis (Gong and Fan, 2010). This indicates that the main sources of phosphorus eutrophication in this area were caused by terrestrial and likely aquaculture input. In addition, active phosphorus (P_{CDB}+OP) is used to characterize the potential phosphorus release from the sediments (Ruban et al., 2001b), the terrestrial sourced P_{CDB} in this study is mostly as high as 50 mg/Kg. Meanwhile, Ex-P is the most active form of phosphorus in sediments as it can easily enter the overlying water (Slomp et al., 1996; Ranjan et al., 2011). The measured bioavailable phosphorus in the sediments was 25.7–

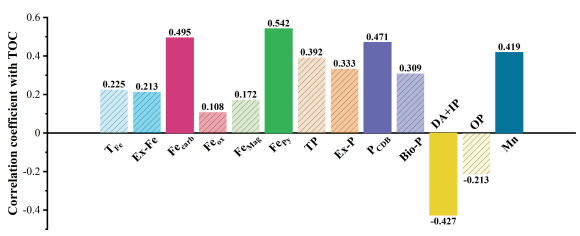

FIGURE 7
Correlation coefficients between different forms of Fe/P/Mn and TOC. The solid bar chart indicated that the variable was significantly correlated with TOC, and the shaded bar chart was not significantly correlated with TOC.

250.6 mg/kg which accounted for 6.10%–47.5% of the TP and indicated significant phosphorus release potential.

It has been revealed that the phosphorus load along the coastal estuaries of China is an important factor for decreasing TOC stability in sediments (Dan et al., 2021). Therefore, investigating the phosphorus load in coastal zones is crucial for accurately assessing the source and sink trend of marine "blue carbon". In the studied coastal sediments, different forms of phosphorus in coastal aquaculture areas correlate differently with TOC. TP and P_{CDB} are positively correlated with TOC, which is consistent with the result reported by Jiang et al. (2014), and the K-means clustering results confirmed that Ex-P, P_{CDB}, and OP can change in the same category as the TOC (Figure 6B). P_{CDB} and OP exhibit high activity and bioavailability (Ruban et al., 2001a; Ruban et al., 2001b; Xie et al., 2011). Previous studies have also confirmed that P_{CDB} has some impact on the eutrophication of overlying water with the alienation of iron oxides (Ruttenberg, 1992), and iron oxides are the main carrier in sediments (Hyacinthe et al., 2006; Fang and Wang, 2021). The phosphorus adsorption capacity gradually decreases with an increase in pH (Shang et al., 1992). In this study, the pH of pore water ranged in 7.45~8.48, P_{CDB} content was thus low in the layers at 10–20, 80–90, and 100–110 cm, where the pH of pore water was higher than 8.00 (Table S1; Figure 5). When the P_{CDB} content is high, the TOC tends to be retained, and vice versa. And P_{CDB}, and Bio-P favored TOC sink due to their high activity and bioavailability on Fe mineral formation.

TOC is negatively correlated with DA+IP (Figure 6A). Studies indicate that DA+IP shares a slight influence of the terrestrial in coastal sediment (Zhou et al., 2016), and it is a crucial P sink refractory in ocean sediment (Ni et al., 2015), which may have a lower tendency to participate in ferric oxyhydroxides transformation than high activity and bioavailability release and re-adsorption P (Chacon et al., 2006; Wen et al., 2023). So we suggested that higher content of DA + IP, and OP indicated TOC source could contribute to sharing the terrestrial's slight influence and a lower tendency to participate in ferric oxyhydroxides transformation.

4.3 Main factors influencing transition from source to sink of TOC

Controlling the TOC sequestration process in sediments is complex. Different speciations of Fe, Mn, P, grain size, and redox conditions are key regulating factors for TOC sequestration (Kothawala et al., 2021; Ma et al., 2022). Most studies have proposed controlling mechanism, which mainly focused on one or a few factors. However, the mechanism coupled with several factors have been hardly discussed. The PLS model is a typical prediction model for the primary and secondary effects of multiple factors on dependent variable changes (Wold et al., 2001). The results showed that PLS had a good predictive fit for TOC (Figure 8B), with a cumulative explanatory variation ratio of TOC as high as 84.5% (Table S3). The factors affecting TOC were ranked according to importance as follows: TIC > clay > Mn > Fe_{Py} > TP >P_{CDB} > TFe> Ex-P >Fe_{Mag} > Bio-P > Fe_{ox}> N > Fe_{carb} > DA+IP > Ex-Fe > OP. Among them, the VIP values of TIC, clay, Mn, P_{CDB}, Fe_{Py}, and TP are all greater than 1, indicating that they are all important factors affecting the occurrence of TOC (Figure 8A). In addition, the PLS model shows a significant negative relationship between Dx(50) and TOC. Clay content has a significant positive relationship with TOC (VIP > 1) (Figure 8), which is consistent with previous studies showing that clay enrichment favors a higher TOC (Gao et al., 2008; Wang et al., 2009). N is significantly positively correlated with TOC, probably due to the direct condensation reaction with TOC, making it difficult for microbe to consume TOC (Janssens et al., 2010).

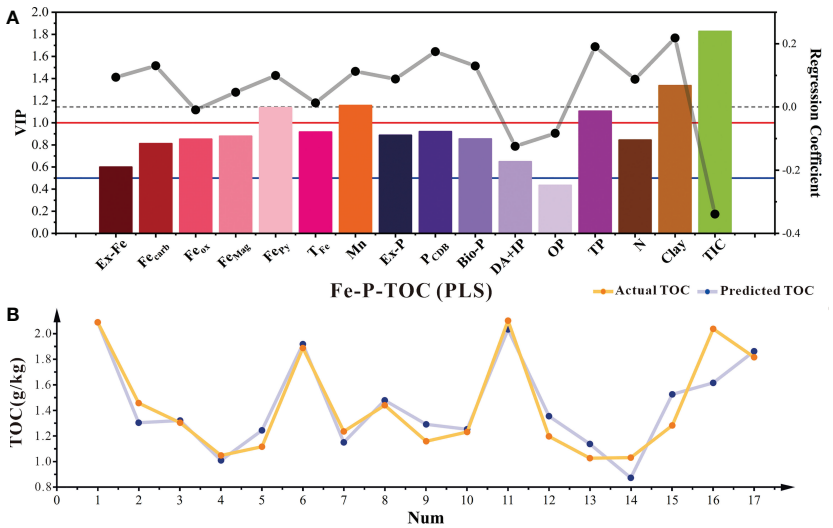

FIGURE 8
PLS model of TOC with different influencing factors in sediments **(A)**. The histogram showed the variable importance of projection (VIP) for each predictive variable; The dot plot showed the regression coefficients of each influence factor. The red solid line, blue solid line, and black dashed line represented different thresholds (VIP=1, VIP=0.5, and RC=0). And the comparison between the predicted results of the PLS model and the actual results **(B)**.

So combining correlation and PLS model prediction results, we suggested that the high contents of Fe_{Py}, Mn, Fe_{Mag}, and Fe_{carb} indicate the conversion of TOC to the sink, which is in accordance with previous studies (Tian et al., 2011; Chalmers and Bustin, 2012; Reithmaier et al., 2020; Li et al., 2021; Zhang et al., 2022). The high Fe_{ox} is also consistent with the conversion of TOC to the source, but the non-siginificant indication of Fe_{ox} on TOC source-sink is due to its abundance relative to TOC content, because only part of Fe_{ox} participates in the oxidation transformation and stable preservation of TOC. For different forms of phosphorus, the high contents of P_{CDB}, Ex-P, and Bio-P represent the transformation of TOC from source to the sink, while the high DA+IP and OP represent the reverse transformation. However, the TP load will lead to the increase of DA+IP and Bio-P simultaneously, the source and sink conversion of TOC could not be directly evaluated here. In addition, Fe_{ox} and P_{CDB} have opposite implications for the source-sink nature of TOC. In the anaerobic iron oxide dissimilated reduction layer, P_{CDB} adsorbed on iron oxides will be released into pore water (Jansson, 1987; Parker and Beck, 2003), and TP eutrophication increases. So, the TOC in the redox transition layer with high Fe_{ox} would convert into the sink. Meanwhile, larger Dx(50) indicates the transformation of TOC to the source, while higher N promote the transformation of TOC to the sink.

5 Conclusions

Iron minerals and phosphates are sensitive factors affecting TOC preservation, but the mechanisms to explain how to effect TOC source-sink transformation still need to be improved. We obtained the following findings. The TFe content was 987.9–2900.7 mg/kg, and Fe_{ox} accounted for 62.2%–79.4%. The TP of the coastal sediments ranged from 337.4–578.0 mg/kg with moderate phosphorus load-release potential, and DA+IP and Bio-P were the leading phosphorus components. Our study suggested that Fe_{carb}, Fe_{Py}, Ex-Fe, Fe_{Mag} have the positive indication for TOC sink mainly associated with symbiosis more iron hydroxide, efficient mineralization, conducive crystallization, and low activity, respectively. While non-significant presentation of Fe_{ox} on TOC source-sink is due to its surplus and strong reactivity. The occurrence of manganese contributed to the TOC deposition due to the strong interaction between Mn(III/IV) minerals and TOC. And P_{CDB}, and Bio-P favored to indicate TOC sink due to their high activity and bioavailability on Fe mineral formation. But higher content of DA+IP, and OP indicated TOC source could be attributed to the slight influence of the terrestrial and lower tendency to participate in ferric oxyhydroxides transformation. Information gained here has important implications for understanding mechanisms and reveals that the control mechanism of TOC environmental occurrence involves the transformation of iron oxide minerals and phosphorus, which forms under the disturbance of human activities.

Data availability statement

The original contributions presented in the study are included in the article/Supplementary Material. Further inquiries can be directed to the corresponding authors.

Author contributions

LG and XL designed the experiments. ZQ, LG, and DC performed all the geochemical experiments and analyzed all the results. ZQ performed the correlation analysis of the Fe-P-TOC model. ZQ and LG prepared the manuscript. XW assisted with the XRF results analysis and part of the language calibration. HL focused on assisting with the SEM experiment and analysis. LG, XL, and YY helped to revise the manuscript. All authors contributed to the article and approved the final submitted version.

Funding

We appreciate the financial support from the National Natural Science Foundation of China (Nos. 41730316, 41902032, 41807351), Key Laboratory of Solid Waste Treatment and Resource Recycling of Ministry of Education (21kfjk04), Interdisciplinary Research Project of Nanjing Normal University (164320H1847), and Nanjing Normal University Talent Training Program (1812200047).

Conflict of interest

The authors declare that the research was conducted in the absence of any commercial or financial relationships that could be construed as a potential conflict of interest.

Publisher's note

Supplementary material

The Supplementary Material for this article can be found online at: https://www.frontiersin.org/articles/10.3389/fmars.2023.1143982/full#supplementary-material

References

Anschutz, P., Bouchet, S., Abril, G., Bridou, R., Tessier, E., and Amouroux, D. (2019). *In vitro* simulation of oscillatory redox conditions in intertidal sediments: N, Mn, fe, and p coupling. *Continental Shelf Res.* 177, 33–41. doi: 10.1016/j.csr.2019.03.007

Arif, M., Ali, S., Ilyas, M., Riaz, M., Akhtar, K., Ali, K., et al. (2021). Enhancing phosphorus availability, soil organic carbon, maize productivity and farm profitability through biochar and organic–inorganic fertilizers in an irrigated maize agroecosystem under semi-arid climate. *Soil Use Management.* 37, 104–119. doi: 10.1111/sum.12661

Bao, Y., Bolan, N. S., Lai, J., Wang, Y., Jin, X., Kirkham, M., et al. (2022). Interactions between organic matter and fe (hydr) oxides and their influences on immobilization and remobilization of metal (loid) s: A review. *Crit. Rev. Environ. Sci. Technol.* 52, 4016–4037. doi: 10.1080/10643389.2021.1974766

Barber, A., Brandes, J., Leri, A., Lalonde, K., Balind, K., Wirick, S., et al. (2017). Preservation of organic matter in marine sediments by inner-sphere interactions with reactive iron. *Sci. Rep.* 7, 1–10. doi: 10.1038/s41598-017-00494-0

Berbel, G. B., Favaro, D. I., and Braga, E. S. (2015). Impact of harbour, industry and sewage on the phosphorus geochemistry of a subtropical estuary in Brazil. *Mar. pollut. bulletin.* 93, 44–52. doi: 10.1016/j.marpolbul.2015.02.016

Boujelben, N., Bouzid, J., Elouear, Z., Feki, M., Jamoussi, F., and Montiel, A. (2008). Phosphorus removal from aqueous solution using iron coated natural and engineered sorbents. *J. hazardous materials.* 151, 103–110. doi: 10.1016/j.jhazmat.2007.05.057

Canfield, D. E. (1989). Reactive iron in marine sediments. *Geochimica Cosmochimica Acta* 53, 619–632. doi: 10.1016/0016-7037(89)90005-7

Canfield, D. E. (1994). Factors influencing organic carbon preservation in marine sediments. *Chem. geology.* 114, 315–329. doi: 10.1016/0009-2541(94)90061-2

Cao, C., Cai, F., Zheng, Y., Wu, C., Lu, H., Bao, J., et al. (2018). Temporal and spatial characteristics of sediment sources on the southern Yangtze shoal over the Holocene. *Sci. Rep.* 8, 1–12. doi: 10.1038/s41598-018-33757-5

Chacon, N., Silver, W. L., Dubinsky, E. A., and Cusack, D. F. (2006). Iron reduction and soil phosphorus solubilization in humid tropical forests soils: The roles of labile carbon pools and an electron shuttle compound. *Biogeochemistry* 78, 67–84. doi: 10.1007/s10533-005-2343-3

Chalmers, G. R. L., and Bustin, R. M. (2012). Geological evaluation of halfway–Doig–Montney hybrid gas shale–tight gas reservoir, northeastern British Columbia. *Mar. Petroleum Geology.* 38, 53–72. doi: 10.1016/j.marpetgeo.2012.08.004

Chen, C., Dynes, J. J., Wang, J., and Sparks, D. L. (2014). Properties of fe-organic matter associations *via* coprecipitation versus adsorption. *Environ. Sci. technology.* 48, 13751–13759. doi: 10.1021/es503669u

Cheng, X., Chen, B., Cui, Y., Sun, D., and Wang, X. (2015). Iron (III) reduction-induced phosphate precipitation during anaerobic digestion of waste activated sludge. *Separation Purification Technol.* 143, 6–11. doi: 10.1016/j.seppur.2015.01.002

Cifuentes, L., Coffin, R., Solorzano, L., Cardenas, W., Espinoza, J., and Twilley, R. (1996). Isotopic and elemental variations of carbon and nitrogen in a mangrove estuary. *Estuarine Coast. Shelf Science.* 43, 781–800. doi: 10.1006/ecss.1996.0103

Dan, S. F., Li, S., Yang, B., Cui, D., Ning, Z., Huang, H., et al. (2021). Influence of sedimentary organic matter sources on the distribution characteristics and preservation status of organic carbon, nitrogen, phosphorus, and biogenic silica in the daya bay, northern south China Sea. *Sci. Total Environment.* 783, 146899. doi: 10.1016/j.scitotenv.2021.146899

Du, J., Liu, K., Huang, J., Han, T., Zhang, L., Anthonio, C. K., et al. (2022). Organic carbon distribution and soil aggregate stability in response to long-term phosphorus addition in different land-use types. *Soil Tillage Res.* 215, 105195. doi: 10.1016/j.still.2021.105195

Du, Y., Ramirez, C. E., and Jaffé, R. (2018). Fractionation of dissolved organic matter by co-precipitation with iron: Effects of composition. *Environ. Processes.* 5, 5–21. doi: 10.1007/s40710-017-0281-4

Fang, T.-H., and Wang, C.-W. (2021). Distribution of geochemical species of p, fe and Mn in surface sediments in the eutrophic estuary, northern Taiwan. *Water* 13, 3075. doi: 10.3390/w13213075

Faust, J. C., Tessin, A., Fisher, B. J., Zindorf, M., Papadaki, S., Hendry, K. R., et al. (2021). Millennial scale persistence of organic carbon bound to iron in Arctic marine sediments. *Nat. Commun.* 12, 1–9. doi: 10.1038/s41467-020-20550-0

Ferguson, J., Burne, R. V., and Chambers, L. A.. (1983). Iron mineralization of peritidal carbonate sediments by continental groundwaters, fisherman bay, South Australia. *Sedimentary Geology* 34 (1), 41–57. doi: 10.1016/0037-0738(83)90034-9

Fookes, P., and Higginbottom, I. (1975). The classification and description of near-shore carbonate sediments for engineering purposes. *Geotechnique* 25, 406–411. doi: 10.1680/geot.1975.25.2.406

Gao, J., Wang, Y., Pan, S., Zhang, R., Li, J., and Bai, F. (2008). Spatial distributions of organic carbon and nitrogen and their isotopic compositions in sediments of the changjiang estuary and its adjacent sea area. *J. Geograph. Sci.* 18, 46–58. doi: 10.1007/s11442-008-0046-0

Giannetta, B., Balint, R., Said-Pullicino, D., Plaza, C., Martin, M., and Zaccone, C. (2020). Fe (II)-catalyzed transformation of fe (oxyhydr) oxides across organic matter fractions in organically amended soils. *Sci. Total Environment.* 748, 141125. doi: 10.1016/j.scitotenv.2020.141125

Golbraikh, A., and Tropsha, A. (2002). Predictive QSAR modeling based on diversity sampling of experimental datasets for the training and test set selection. *J. Computer-Aided Mol. Design.* 16, 357–369. doi: 10.1023/A:1020869118689

Gong, C. S., and Fan, C. X. (2010). Effect factors analysis of phosphorus exchange across lake sediment-water interface under different dissolved oxygen concentration (in Chinese). *Journal of Lake Sciences* 22, 430–436. doi: 10.18307/2010.0317

Hartnett, H. E., Keil, R. G., Hedges, J. I., and Devol, A. H. (1998). Influence of oxygen exposure time on organic carbon preservation in continental margin sediments. *Nature* 391, 572–575. doi: 10.1038/35351

Hedges, J. I., and Keil, R. G. (1995). Sedimentary organic matter preservation: An assessment and speculative synthesis. *Mar. Chem.* 49, 81–115. doi: 10.1016/0304-4203(95)00008-F

Hemingway, J. D., Rothman, D. H., Grant, K. E., Rosengard, S. Z., Eglinton, T. I., Derry, L. A., et al. (2019). Mineral protection regulates long-term global preservation of natural organic carbon. *Nature* 570, 228–231. doi: 10.1038/s41586-019-1280-6

Hermans, M., Astudillo Pascual, M., Behrends, T., Lenstra, W. K., Conley, D. J., and Slomp, C. P. (2021). Coupled dynamics of iron, manganese, and phosphorus in brackish coastal sediments populated by cable bacteria. *Limnol. Oceanogr.* 66, 2611–2631. doi: 10.1002/lno.11776

Huang, J., Hu, B., Qi, K., Chen, W., Pang, X., Bao, W., et al. (2016). Effects of phosphorus addition on soil microbial biomass and community composition in a subalpine spruce plantation. *Eur. J. Soil Biol.* 72, 35–41. doi: 10.1016/j.ejsobi.2015.12.007

Hyacinthe, C., Bonneville, S., and Cappellen, P. V. (2006). Reactive iron(III) in sediments: Chemical versus microbial extractions. *Geochimica Cosmochimica Acta* 70, 4166–4180. doi: 10.1016/j.gca.2006.05.018

Janssens, I. A., Dieleman, W. I. J., Luyssaert, S., Subke, J. A., Reichstein, M., Ceulemans, R., et al. (2010). Reduction of forest soil respiration in response to nitrogen deposition. *Nat. Geosci.* 3, 315–322. doi: 10.1038/ngeo844

Jansson, M. (1987). Anaerobic dissolution of iron-phosphorus complexes in sediment due to the activity of nitrate-reducing bacteria. *Microbial Ecol.* 14, 81–89. doi: 10.1007/BF02011573

Jiang, S., Lin, P., Lin, J., Cai, J., Xu, Y., and Zheng, L. (2014). Distribution characteristics of phosphorus and its environmental significance in the surface sediments of xiamen gulf (in Chinese). *J. Of Trop. Oceanogr.* 33, 72–78. doi: 10.11978/j.issn.1009-5470.2014.03.011

Jiao, N., Herndl, G. J., Hansell, D. A., Benner, R., Kattner, G., Wilhelm, S. W., et al. (2010). Microbial production of recalcitrant dissolved organic matter: Long-term carbon storage in the global ocean. *Nat. Rev. Microbiol.* 8, 593–599. doi: 10.1038/nrmicro2386

Jiao, N., Robinson, C., Azam, F., Thomas, H., Baltar, F., Dang, H., et al. (2014). Mechanisms of microbial carbon sequestration in the ocean–future research directions. *Biogeosciences* 11, 5285–5306. doi: 10.5194/bg-11-5285-2014

Johnson, K., Purvis, G., Lopez-Capel, E., Peacock, C., Gray, N., Wagner, T., et al. (2015). Towards a mechanistic understanding of carbon stabilization in manganese oxides. *Nat. Commun.* 6, 1–11. doi: 10.1038/ncomms8628

Kerr, G., Craw, D., Trumm, D., and Pope, J. (2018). Authigenic realgar and gold in dynamic redox gradients developed on historic mine wastes, new Zealand. *Appl. Geochemistry.* 97, 123–133. doi: 10.1016/j.apgeochem.2018.08.009

Kleber, M., Bourg, I. C., Coward, E. K., Hansel, C. M., Myneni, S. C., and Nunan, N. (2021). Dynamic interactions at the mineral–organic matter interface. *Nat. Rev. Earth Environment.* 2, 402–421. doi: 10.1038/s43017-021-00162-y

Kontny, A., Schneider, M., Eiche, E., Stopelli, E., Glodowska, M., Rathi, B., et al. (2021). Iron mineral transformations and their impact on as (im)mobilization at redox interfaces in as-contaminated aquifers. *Geochimica Et Cosmochimica Acta* 296, 189–209. doi: 10.1016/j.gca.2020.12.029

Kothawala, D. N., Kellerman, A. M., Catalán, N., and Tranvik, L. J. (2021). Organic matter degradation across ecosystem boundaries: The need for a unified conceptualization. *Trends Ecol. Evolution.* 36, 113–122. doi: 10.1016/j.tree.2020.10.006

Krom, M. D., Mortimer, R. J., Poulton, S. W., Hayes, P., Davies, I. M., Davison, W., et al. (2002). In-situ determination of dissolved iron production in recent marine sediments. *Aquat. Sci.* 64, 282. doi: 10.1007/s00027-002-8072-y

Lalonde, K., Mucci, A., Ouellet, A., and Gélinas, Y. (2012). Preservation of organic matter in sediments promoted by iron. *Nature* 483, 198–200. doi: 10.1038/nature10855

Lapointe, B. E., Littler, M. M., and Littler, D. S. (1992). Nutrient availability to marine macroalgae in siliciclastic versus carbonate-rich coastal waters. *Estuaries* 15, 75–82. doi: 10.2307/1352712

Li, Q., Hu, W., Li, L., and Li, Y. (2023). Interactions between organic matter and fe oxides at soil micro-interfaces: Quantification, associations, and influencing factors. *Sci. Total Environ.* 855, 158710. doi: 10.1016/j.scitotenv.2022.158710

Li, H., Santos, F., Butler, K., and Herndon, E. (2021). A critical review on the multiple roles of manganese in stabilizing and destabilizing soil organic matter. *Environ. Sci. Technol.* 55, 12136–12152. doi: 10.1021/acs.est.1c00299

Li, T., Zhong, W., Jing, C., Li, X., Zhang, T., Jiang, C., et al. (2020). Enhanced hydrolysis of p-nitrophenyl phosphate by iron (hydr) oxide nanoparticles: Roles of exposed facets. *Environ. Sci. Technol.* 54, 8658–8667. doi: 10.1021/acs.est.9b07473

Liu, H., Shu, D., Sun, F., Li, Q., Chen, T., Xing, B., et al. (2019). Effect of manganese substitution on the crystal structure and decomposition kinetics of siderite. *J. Thermal Anal. Calorimetry.* 136, 1315–1322. doi: 10.1007/s10973-018-7767-9

Lovley, D. R. (1991). Dissimilatory Fe(III) and Mn(IV) reduction. *Microbiol. Rev.* 55, 259–287. doi: 10.1128/mr.55.2.259-287.1991

Ma, W.-W., Zhu, M.-X., Yang, G.-P., and Li, T. (2018). Iron geochemistry and organic carbon preservation by iron (oxyhydr) oxides in surface sediments of the East China Sea and the south yellow Sea. *J. Mar. Syst.* 178, 62–74. doi: 10.1016/j.jmarsys.2017.10.009

Ma, W.-W., Zhu, M.-X., Yang, G.-P., Li, T., Li, Q.-Q., Liu, S.-H., et al. (2022). Stability and molecular fractionation of ferrihydrite-bound organic carbon during iron reduction by dissolved sulfide. *Chem. Geology.* 594, 120774. doi: 10.1016/j.chemgeo.2022.120774

Macreadie, P. I., Anton, A., Raven, J. A., Beaumont, N., Connolly, R. M., Friess, D. A., et al. (2019). The future of blue carbon science. *Nat. Commun.* 10, 3998. doi: 10.1038/s41467-019-11693-w

Macreadie, P. I., Costa, M. D., Atwood, T. B., Friess, D. A., Kelleway, J. J., Kennedy, H., et al. (2021). Blue carbon as a natural climate solution. *Nat. Rev. Earth Environment.* 2, 826–839. doi: 10.1038/s43017-021-00224-1

Mao, X., Van Zwieten, L., Zhang, M., Qiu, Z., Yao, Y., and Wang, H. (2020). Soil parent material controls organic matter stocks and retention patterns in subtropical China. *J. Soils Sediments.* 20, 2426–2438. doi: 10.1007/s11368-020-02578-3

März, C., Riedinger, N., Sena, C., and Kasten, S. (2018). Phosphorus dynamics around the sulphate-methane transition in continental margin sediments: Authigenic apatite and fe (II) phosphates. *Mar. Geology.* 404, 84–96. doi: 10.1016/j.margeo.2018.07.010

Nakamura, J., Lall, U., Kushnir, Y., and Camargo, S. J. (2009). Classifying north Atlantic tropical cyclone tracks by mass moments. *J. Climate.* 22, 5481–5494. doi: 10.1175/2009JCLI2828.1

Ni, J., Lin, P., Zhen, Y., Yao, X., and Guo, L. (2015). Distribution, source and chemical speciation of phosphorus in surface sediments of the central pacific ocean. *Deep Sea Res. Part I: Oceanograph. Res. Pap.* 105, 74–82. doi: 10.1016/j.dsr.2015.08.008

O'loughlin, E. J., Gorski, C. A., and Scherer, M. (2015). Effects of phosphate on secondary mineral formation during the bioreduction of akaganeite (β-FeOOH): Green rust versus framboidal magnetite. *Curr. Inorganic Chem.* 5, 214–224. doi: 10.2174/1877944105666150421001126

Parker, A. K., and Beck, M. B. (2003). Iron reduction and phosphorus release from lake sediments and bt horizon soil: Incubation studies to explore phosphorus cycling. Georia Tech. Available at: http://hdl.handle.net/1853/48363.

Pasakarnis, T., Mccormick, M. L., Parkin, G. F., Thompson, A., and Scherer, M. M. (2014). FeIIaq–FeIIIoxide electron transfer and fe exchange: Effect of organic carbon. *Environ. Chem.* 12, 52–63. doi: 10.1071/EN14035

Poulton, S. W., and Canfield, D. E. (2005). Development of a sequential extraction procedure for iron: Implications for iron partitioning in continentally derived particulates. *Chem. Geology.* 214, 209–221. doi: 10.1016/j.chemgeo.2004.09.003

R Core Team. (2022). *R: A language and environment for statistical computing.* R Foundation for Statistical Computing, Vienna, Austria. Available at: https://www.R-project.org/.

Raiswell, R., and Canfield, D. E. (1998). Sources of iron for pyrite formation in marine sediments. *Am. J. Science.* 298, 219–245. doi: 10.2475/ajs.298.3.219

Ranjan, R. K., Ramanathan, A., Chauhan, R., and Singh, G. (2011). Phosphorus fractionation in sediments of the pichavaram mangrove ecosystem, south-eastern coast of India. *Environ. Earth Sci.* 62, 1779–1787. doi: 10.1007/s12665-010-0659-3

Reichenbach, M., Fiener, P., Hoyt, A., Trumbore, S., Six, J., and Doetterl, S. (2023). Soil carbon stocks in stable tropical landforms are dominated by geochemical controls and not by land use. *Global Change Biol.* 00, 1–17. doi: 10.1111/gcb.16622

Reithmaier, G. M. S., Johnston, S. G., Junginger, T., Goddard, M. M., Sanders, C. J., Hutley, L. B., et al. (2021). Alkalinity production coupled to pyrite formation represents an unaccounted blue carbon sink. *Global Biogeochem. Cycles* 35, e2020GB006785. doi: 10.1029/2020GB006785

Ruban, V., Lopez-Sanchez, J. F., Pardo, P., Rauret, G., Muntau, H., and Quevauviller, P. (2001a). Development of a harmonised phosphorus extraction procedure and certification of a sediment reference material. *J. Environ. Monitoring.* 3, 121–125. doi: 10.1039/b005672n

Ruban, V., Lopez-Sanchez, J. F., Pardo, P., Rauret, G., Muntau, H., and Quevauviller, P. (2001b). Harmonized protocol and certified reference material for the determination of extractable contents of phosphorus in freshwater sediments - a synthesis of recent works. *Fresenius J. Analytical Chem.* 370, 224–228. doi: 10.1007/s002160100753

Ruttenberg, K. C. (1992). Development of a sequential extraction method for different forms of phosphorus in marine sediments. *Limnol. Oceanogr.* 37, 1460–1482. doi: 10.4319/lo.1992.37.7.1460

Sarkar, B., Singh, M., Mandal, S., Churchman, G. J., and Bolan, N. S. (2018). Clay minerals–organic matter interactions in relation to carbon stabilization in soils. *Future Soil carbon.* 4, 71–86. doi: 10.1016/B978-0-12-811687-6.00003-1

Schad, M., Halama, M., Jakus, N., Robbins, L. J., Warchola, T. J., Tejada, J., et al. (2021). Phosphate remobilization from banded iron formations during metamorphic mineral transformations. *Chem. Geology.* 584, 120489. doi: 10.1016/j.chemgeo.2021.120489

Shang, C., Stewart, J. W. B., and Huang, P. M. (1992). pH effect on kinetics of adsorption of organic and inorganic phosphates by short-range ordered aluminum and iron precipitates. *Geoderma* 53, 1–14. doi: 10.1016/0016-7061(92)90017-2

Shi, J., Gong, J., Li, X., Zhang, Z., Zhang, W., Li, Y., et al. (2022). Plant–microbial linkages regulate soil organic carbon dynamics under phosphorus application in a typical temperate grassland in northern China. *Agriculture Ecosyst. Environment.* 335, 108006. doi: 10.1016/j.agee.2022.108006

Shi, Z., Huang, X. D., Ai, L., Fang, N., and Wu, G. (2014). Quantitative analysis of factors controlling sediment yield in mountainous watersheds. *Geomorphology* 226, 193–201. doi: 10.1016/j.geomorph.2014.08.012

Singh, P., Udayana, S. K., Mukherjee, S., Jaison, M., Das, B. P., and Mehjabeen, (2021). Nutrient biogeochemistry of coastal soils. *Pharma Innovation.* 10, 972–976. Available at: https://www.thepharmajournal.com/archives/?year=2021&vol=10&issue=7&ArticleId=6983.

Slomp, C. P., Epping, E. H. G., Helder, W., and Raaphorst, W. V. (1996). A key role for iron-bound phosphorus in authigenic apatite formation in north Atlantic continental platform sediments. *J. Mar. Res.* 54, 1179–1205. doi: 10.1357/0022240963213745

Smith, V. H., and Schindler, D. W. (2009). Eutrophication science: Where do we go from here? *Trends Ecol. evolution.* 24, 201–207. doi: 10.1016/j.tree.2008.11.009

Sweeney, R., and Kaplan, I. (1973). Pyrite framboid formation; laboratory synthesis and marine sediments. *Economic Geology.* 68, 618–634. doi: 10.2113/gsecongeo.68.5.618

Tang, J., Ye, S., Chen, X., Yang, H., Sun, X., Wang, F., et al. (2018). Coastal blue carbon: Concept, study method, and the application to ecological restoration. *Sci. China Earth Sci.* 61, 637–646. doi: 10.1007/s11430-017-9181-x

Thamdrup, B. (2000). Bacterial manganese and iron reduction in aquatic sediments. *Adv. Microbial Ecol.* 16, 41–84. doi: 10.1007/978-1-4615-4187-5_2

Tian, Q., Yang, T., Zhang, S., Shi, P., Zhang, J., and Fan, Z. (2011). Magnetic susceptibility and its environmental significance of lake sediments in Tibet plateau (in Chinese). *Acta Sedimentol. Sinica.* 29, 143–150. doi: 10.14027/j.cnki.cjxb.2011.01.011

Trefethen, J. M. (1950). Classification of sediments. *Am. J. Science.* 248, (1) 55–(1) 62. doi: 10.2475/ajs.248.1.55

Treude, T., Krause, S., Maltby, J., Dale, A. W., Coffin, R., and Hamdan, L. J. (2014). Sulfate reduction and methane oxidation activity below the sulfate-methane transition zone in alaskan Beaufort Sea continental margin sediments: Implications for deep sulfur cycling. *Geochimica Cosmochimica Acta* 144, 217–237. doi: 10.1016/j.gca.2014.08.018

Wan, B., Yang, P., Jung, H., Zhu, M., Diaz, J. M., and Tang, Y. (2021). Iron oxides catalyze the hydrolysis of polyphosphate and precipitation of calcium phosphate minerals. *Geochimica Cosmochimica Acta* 305, 49–65. doi: 10.1016/j.gca.2021.04.031

Wang, B., Lei, H., and Huang, F. (2022). Impacts of sulfate-driven anaerobic oxidation of methane on the morphology, sulfur isotope, and trace element content of authigenic pyrite in marine sediments of the northern south China Sea. *Mar. Petroleum Geology.* 139, 105578. doi: 10.1016/j.marpetgeo.2022.105578

Wang, H., Xiao, C., Li, C., Li, Y., Zhang, W., Fu, X., et al. (2009). Spatial variability of organic carbon in the soil of wetlands in chongming dongtan and its influential factors (in Chinese). *J. Agro-Environment Science.* 28, 1522–1528. Available at: https://kns.cnki.net/kcms2/article/abstract?v=pbgqCeizVJPi8XOORhwDuKDIU5yDlOn4vsQkmJn_xC6GeIEDVS8lTPFaVSG2cfBfjFaOUOmMtHVfN0oWDzHJ_FJ9_Fih_AyP0vaJ9D3wce4AKweHvlYBg==&uniplatform=NZKPT&language=CHS.

Wen, S., Lu, Y., Dai, J., Huang, X., An, S., Liu, J., et al. (2023). Stability of organic matter-iron-phosphate associations during abiotic reduction of iron. *J. Hazardous Materials* 449, 131016. doi: 10.1016/j.jhazmat.2023.131016

Wen, H., Zheng, R., Geng, W., Fan, M., and Wang, M. (2007). Characteristics of rare earth elements of lacustrine exhalative rock in the xiagou formation of lower Cretaceous in qingxi sag, jiuxi basin. *Front. Earth Sci. China.* 1, 333–340. doi: 10.1007/s11707-007-0040-3

Weng, L., Van Riemsdijk, W. H., and Hiemstra, T. (2012). Factors controlling phosphate interaction with iron oxides. *J. Environ. quality.* 41, 628–635. doi: 10.2134/jeq2011.0250

Wold, S. (1995). PLS for multivariate linear modeling. In *Chemometric Methods Mol. Design, Methods and Principles in Medicinal Chemistry* 2, 195–218. doi: 10.1002/9783527615452.ch4

Wold, S., Sjöström, M., and Eriksson, L. (2001). PLS-regression: A basic tool of chemometrics. *Chemometrics Intelligent Lab. Syst.* 58, 109–130. doi: 10.1016/S0169-7439(01)00155-1

Xia, S., Song, Z., Van Zwieten, L., Guo, L., Yu, C., Wang, W., et al. (2022). Storage, patterns and influencing factors for soil organic carbon in coastal wetlands of China. *Global Change Biol.* 28, 6065–6085. doi: 10.1111/gcb.16325

Xie, C., Tang, J., Zhao, J., Wu, D., and Xu, X. (2011). Comparison of phosphorus fractions and alkaline phosphatase activity in sludge, soils, and sediments. *J. Soils Sediments.* 11, 1432–1439. doi: 10.1007/s11368-011-0429-1

Xu, X., Shi, R., Lv, C.-Y., Liu, H., Yang, W., Qian, S., et al. (2021). Hydrodynamic-driven changes in the source and composition of sedimentary organic matter *via* grain size distribution in shallow lakes. *J. Geophys. Res.: Biogeosci.* 126, e2021JG006502. doi: 10.1029/2021JG006502

Yalcin, M. G., Nyamsari, D., Ozer Atakoglu, O., and Yalcin, F. (2022). Chemical and statistical characterization of beach sand sediments: Implication for natural and anthropogenic origin and paleo-environment. *Int. J. Environ. Sci. Technol.* 19, 1335–1356. doi: 10.1007/s13762-021-03280-8

Yan, X., Yang, W., Muneer, M. A., Zhang, S., Wang, M., and Wu, L. (2021). Land-use change affects stoichiometric patterns of soil organic carbon, nitrogen, and phosphorus in the red soil of southeast China. *J. Soils Sediments.* 21, 2639–2649. doi: 10.1007/s11368-021-02953-8

Yoon, S.-Y., Lee, C.-G., Park, J.-A., Kim, J.-H., Kim, S.-B., Lee, S.-H., et al. (2014). Kinetic, equilibrium and thermodynamic studies for phosphate adsorption to magnetic iron oxide nanoparticles. *Chem. Eng. J.* 236, 341–347. doi: 10.1016/j.cej.2013.09.053

Zhang, C., Xiao, Q., Sun, P. A., Gao, X., Guo, Y., Miao, Y., et al. (2022). Progress on karst carbon cycle and carbon sink effect study and perspective. *Bull. Geol. Sci. Technol.* 41, 190–198. doi: 10.19509/j.cnki.dzkq.2022.0193

Zhang, Y., Zhao, M., Cui, Q., Fan, W., Qi, J., Chen, Y., et al. (2017). Processes of coastal ecosystem carbon sequestration and approaches for increasing carbon sink. *Sci. China Earth Sci.* 60, 809–820. doi: 10.1007/s11430-016-9010-9

Zhao, M., Mills, B. J., Homoky, W. B., and Peacock, C. L. (2023). Oxygenation of the earth aided by mineral–organic carbon preservation. *Nat. Geosci.* 16, 262–267. doi: 10.1038/s41561-023-01133-2

Zhao, Y., Moore, O. W., Xiao, K.-Q., Curti, L., Fariña, A. O., Banwart, S. A., et al. (2022). The role and fate of organic carbon during aging of ferrihydrite. *Geochimica Cosmochimica Acta* 335, 339–355. doi: 10.1016/j.gca.2022.07.003

Zhou, F., Gao, X., Yuan, H., Song, J., Chen, C.-T. A., Lui, H.-K., et al. (2016). Geochemical forms and seasonal variations of phosphorus in surface sediments of the East China Sea shelf. *J. Mar. Syst.* 159, 41–54. doi: 10.1016/j.jmarsys.2016.03.005